XLIII CILAMCE
21–25, November, 2022
FOZ DO IGUAÇU – PR – BRAZIL

Geomechanical damage evaluation of fractured carbonate rocks scenarios related to the Brazilian Pre-salt via finite element analysis

Ximena A. Rodríguez Flórez[1], Leonardo J. Guimarães[1], Bruno M. Canabarro[1]

[1]*Dept. of Civil Engineering, Federal University of Pernambuco*
Av. da Arquitetura - Cidade Universitária, 50740-540, Recife/PE, Brasil
ximena.florez@ufpe.br, leonardo.guimaraes@ufpe.br, bruno.canabarro@ufpe.br

Abstract. The structural configuration of the Brazilian Pre-salt oil system took place in a Rift tectonic formation environment. The presence of faults, joints, breccias, fractures, and microfractures makes the system complex. Natural discontinuities impact reservoir fluid production because they may be a highly conductive primary flow pathway in naturally fractured reservoirs. Several factors affect the pathway conductivity, such as the fracture's state, size, stiffness, and geometry. Moreover, fluid-rock interaction also controls the reservoir fluid production dynamics due to the hydro-mechanical effects. Our work analyzes the geomechanical behavior of fractures in naturally fractured carbonate reservoirs. We apply finite elements methods (FEM), the embedded strong discontinuities methodology, and Barton's constitutive model. The methodology discretizes coarser meshes in the domain and shows the impact of the fracture aperture as a function of the normal fracture stiffness. The results show that initial fracture normal stiffness directly impacts the fracture deformability during production, especially near the wellbore.

Keywords: embedded strong discontinuities, normal fracture stiffness, hydro-mechanical coupling.

1 Introduction

Carbonate reservoirs are economically important in the oil and gas industry because they hold a significant portion of the world's oil and gas reserves. The oil zone is located below a salt layer that can reach up to 3000 meters of thickness, a distance from the coast of approximately 300 km, and a water depth up to 5000 meters [1]. This province comprises significant accumulations of excellent quality and commercially valuable light oil [2].

A naturally fractured reservoir under the state of in-situ stress corresponds to a system in equilibrium conditions. The formation's stress state changes during the drilling of a well hole in the system. Replacing the rock system by drilling fluids increases the stress anisotropy at the wellbore face and changes the intrinsic properties of the rock and the fluids it contains [3], [4]. The redistribution of stresses around the wellbore can lead to the closure of the fracture, reducing reservoir permeability. Understanding the behavior between matrix, fracture, and fluids in this stress-sensitive reservoir during production/injection may help keep the productivity over time. Numerous studies have developed analytical, experimental, and numerical models to evaluate the fracture deformation performance during fluid production. The models consider variables like principal stresses, effective normal stress, shear stress, rock properties, and fracture properties (i.e., compressibility, stiffness, frequency, aperture, and closure mechanism) [5]–[7]. Goodman [8], introduces the term "normal stiffness" of the fracture, which describes the variation in the rate of normal stress as a function of the normal displacements. Subsequently, Bandis et al. [7], expose some experimental studies showing the variation of fracture deformability under normal and shear stresses. Thus, the authors suggest a hyperbolic function to describe the relationship between stress and aperture/closure of the fractures. Fracture normal stiffness is part of studies to analyze fracture´s deformability. Even so, studies do not include the impact in the relation reservoir production - fracture normal stiffness. For this reason, this study

integrates efficient simulation methodologies with Barton's constitutive model [7] to analyze the impact of the initial fracture stiffness on the reduction of permeability due to the closure of the fractures.

2 Numerical fracture model

The embedded strong discontinuities are a method applied to numerical modeling using finite elements. This method allows the simulation of a porous medium fracture. The approach is an efficient technique to analyze the deformability of the fractures in different production/injection scenarios as evidenced in the following works [9]–[12]. Finite element methods, embedded discontinuities technique, and the Barton-Bandis constitutive model are integrated to evaluate the impact of the normal fracture stiffness and fracture closure on reservoir fluid production. The numerical development of the model was implemented in the simulator *CODE_BRIGHT* (*Coupled Deformation Brine Gas and heat Transport*) [13], [14]. The *CODE_BRIGHT* has been adapted to resolve the numerical fracture model applying the mentioned methodologies [9], [10], [15]. The simulator *CODE_BRIGHT* solves the hydraulic and mechanical problem in a coupled way. The equations are solved for all elements of the mesh. The unknows for hydraulic and mechanical problem are pressure and displacements, respectively.

2.1 Embedded discontinuities in finite elements methods

The finite elements methods are used to describe the continuous part. Beserra [9], [12] exposes the discontinuity behavior in the interface can be described by a constitutive equation with a relation between stresses and displacements (discrete model) or with a constitutive model relates stresses and strain. Manzoli [11], introduces a new continuous approximation of strong discontinuities including the effect of band strain on existing elements. Consider a solid of domain Ω and boundary Γ as shown in Figure 1a. The boundary Γ is composed by the boundary depending on the prescribed stress Γ_t and the boundary relating with displacements Γ_u.

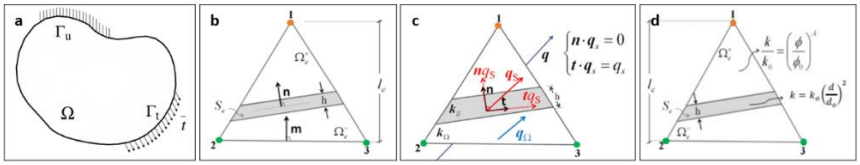

Figure 1. a- Domain of equilibrium problem, [9]. b- Discontinuity band in a finite element, [9]. c- Flow vector (q_S) decomposition: normal component nq_S and tangencial component (tq_S),[9]. d- Laws for permeability variations in continuum and discontinue medium, [9].

Figure 1b shows a finite element with three nodes. The element has a dominium Ω_e and a lenght l_e. The strain band (S_e) have a widht (h) that break down the element in two parts. So, the node 1 is separated of the others. The displacement field of an element ($\boldsymbol{u}$) can be divided in two components (u_Ω and u_S). u_Ω is related with the continium strain and u_S is related to rigid motion inside the element. Thus, displacement field of an element can be written as eq. (1). Equations (2) and (3) describe the strain in the continues and discontinues part. Where $\boldsymbol{\varepsilon}_\Omega$ is the strain in the continuun and $\boldsymbol{\varepsilon}_S$ is he strain in the discontinuity. $[\![\boldsymbol{u}]\!]$ represents the jump in the displacement field. $\boldsymbol{M}$ and $\boldsymbol{N}$ are matrix with the $\boldsymbol{m}$ and $\boldsymbol{n}$ vectors components (Figure 1b).

$$\boldsymbol{u} = u_\Omega + u_S \tag{1}$$

$$\boldsymbol{\varepsilon}_\Omega = \boldsymbol{\varepsilon} - \frac{1}{l_e}\boldsymbol{M}[\![\boldsymbol{u}]\!] \tag{2}$$

$$\boldsymbol{\varepsilon}_S = \boldsymbol{\varepsilon} - \frac{1}{l_e}\boldsymbol{M}[\![\boldsymbol{u}]\!] + \frac{1}{h}\boldsymbol{N}[\![\boldsymbol{u}]\!] \tag{3}$$

The continuous part is considered elastic-linear and isotropic. Then, the corresponding stress field in the continuum ($\boldsymbol{\sigma}_\Omega$) and discontinium ($\boldsymbol{\sigma}_S$) part can be written as show in eq. (4) and (5). The continuity of stresses in the interface between the discontinuity band and the element continuous part can be written as eq. (6). $\boldsymbol{n}$ is the normal vector of the discontinuity plane.

$$\boldsymbol{\sigma}_\Omega = \Sigma\,(\varepsilon_\Omega) = \Sigma\left(\boldsymbol{\varepsilon} - \frac{1}{l_e}\boldsymbol{M}[\![\boldsymbol{u}]\!]\right) \tag{4}$$

$$\boldsymbol{\sigma}_{\mathrm{S}} = \Sigma\left(\varepsilon_{\mathrm{S}}\right) = \Sigma\left(\boldsymbol{\varepsilon} - \frac{1}{l_e}\boldsymbol{M}[\![\boldsymbol{u}]\!] + \frac{1}{h}\boldsymbol{N}[\![\boldsymbol{u}]\!]\right) \tag{5}$$

$$\boldsymbol{n}\,.\left(\boldsymbol{\sigma}_{\Omega} - \boldsymbol{\sigma}_{\mathrm{S}}\right) = 0 \tag{6}$$

2.2 Closure fracture constitutive model

The constitutive model implemented is Barton-Bandis closure model [7]. The model corresponds with a hyperbolic model that represent the mechanical behavior of the fractured medium. The model is a nonlinear elastic model used to study the fracture closure under normal compressive stresses. The normal stress on the fracture is described as eq. (7). Barton-Bandis model describes numerically the normal closure as eq. (8). Then, the displacement jump vector can be written as eq. (9). The discontinuity strain field is given by eq. (10). $\boldsymbol{\varepsilon}^0{}_S$ corresponds with the in-situ strain field in the discontinuity.

$$\sigma_n = \boldsymbol{n}\,.\,\boldsymbol{\sigma}_S\,.\,\boldsymbol{n} \tag{7}$$

$$j = \frac{\sigma_n V_m}{\sigma_n - K_{ni} V_m} \tag{8}$$

$$[\![\boldsymbol{u}]\!] = j\,\boldsymbol{n} \tag{9}$$

$$\boldsymbol{\varepsilon}_{\mathrm{S}} = \boldsymbol{\varepsilon} - \frac{1}{l_e}\boldsymbol{M}[\![\boldsymbol{u}]\!] + \frac{1}{h}\boldsymbol{N}[\![\boldsymbol{u}]\!] + \boldsymbol{\varepsilon}^0{}_S \tag{10}$$

2.3 Fluid flow fractures problem

The Darcy's flow through the fracture is decomposed in normal and tangential component. There is not fluid flow at the interface between the discontinuity and the continuous part [9]–[11], [16]. So, the Fluid flow Darcy's law for a continuum ($\boldsymbol{q}_{\Omega}$) and discontinue ($\boldsymbol{q}_{\mathrm{S}}$) part can be written as eq. (11) and (12). $\boldsymbol{K}_{\Omega}$ and K_S are the tensor of the permeability in the continuum and discontinue part, respectively. Specifically, K_S represents the intrinsic fracture permeability. ∇P is the pressure gradient and *t* is the vector that defines the direction of the discontinuity.

$$\boldsymbol{q}_{\Omega} = -\boldsymbol{K}_{\Omega}\,\nabla P \tag{11}$$

$$\boldsymbol{q}_S = -\frac{h}{l_e} K_S\,\boldsymbol{t}\otimes\boldsymbol{t}\,\nabla P \tag{12}$$

Figure 1c shows the normal and tangential component of the flow vector into the discontinuity band. A discontinuity in a porous medium corresponds with the preferential flow pathway. A permeability anisotropy is considered. Thus, the higher permeability is assumed in the direction of the fracture. Equations (13) and (14) describes the effective permeability tensor ($\boldsymbol{K}_{ef}$) that incorporates the permeability anisotropy generated by the preferential flow channel of the discontinuity.

$$\boldsymbol{q} = -\boldsymbol{K}_{ef}\,\nabla P \tag{13}$$

$$\boldsymbol{K}_{ef} = \left(\boldsymbol{K}_{\Omega} + \frac{h}{l_e} + K_S\,\boldsymbol{t}\otimes\boldsymbol{t}\right) \tag{14}$$

2.4 Permeability of the continuum and discontinue medium

The permeability quadratic law is implemented to calculate the rock permeability (see Figure 1d). The rock permeability (k_m) is given by eq. (15). k_0 represents the initial rock permeability. φ_0 represents the initial porosity. φ corresponds with the porosity calculated due stress and strain changes. *A* is an exponent that needs to be calculated experimentally. On the other hand, Navier Stokes equation describes the permeability of a discontinuity for a flow in a single opening fracture with a constant width (*h*), between two parallel planes, eq. (16). The fracture aperture is calculated as a function of the displacement jump field from the discontinuity. Thus, the fracture aperture can be expressed as eq. (17).

$$k_m = k_0\left(\frac{\varphi}{\varphi_0}\right)^A \tag{15}$$

$$k_S = \frac{h^2}{12} \tag{16}$$

$$h = V_m - j \tag{17}$$

3 Study case: Brazilian Pre-salt

Numerical simulations were worked with data from a naturally fractured carbonate rocks from the Brazilian Pre-salt. Table 1 shows the rock and fracture properties implemented in the simulations. The computational cells used in this work have a size of 200x200 m. The numerical simulations were carried under oedometric conditions under a fixed confining vertical stress (S_v). The reservoir is depleted due to production, until get the wellbore pressure, to analyze the behavior of the fracture closure.

Table 1 shows the used rock and fracture properties in the simulations.

Table 1 - Rock and fracture properties of the study case. Source: author

Property	***Value***	***Unit***	***Symbol***
Rock permeability	3.388e-14	m^2	k_m
Rock porosity	0.0758		φ_m
Biot's coefficient	1		α
Young's Modulus	1.69e4	MPa	E
Poisson ratio	0.3		v
Initial fracture normal stiffness	12,041e3	MPa/m	K_{ni}
Initial reservoir pressure	55	MPa	P_i
Wellbore pressure	10	MPa	P_w
Vertical stress	100	MPa	S_v
Fluid viscosity	1e-9	MPa/s	μ

4 Analysis of results

The impact of the K_{ni} on the fracture aperture is evaluated comparing the simulations results obtained with different K_{ni}. A lower K_{ni} and a higher K_{ni} respect to the Pre-salt reference value (12,041 MPa/m) are considered in the analysis. The proposed K_{ni} data are taken from the experiments presented in [7]. The implemented values correspond to K_{ni} values of a carbonate rock in a degraded to semi-degraded state. K_{ni} values for this study were 3,800 MPa/m and 65,000 MPa/m. The relation between the initial normal stiffness and the geomechanical damage due to fracture closure is analyzed at a global and local level. The global level is referring to a reservoir scale and the local scale corresponds with some punctual fractures.

4.1 Global impact to the K_{ni} on the reservoir production

Figure 2 shows the evolution of the maximum cumulative production as a function of time for the different k_{ni} values. The case with 75 fractures describes an increase in the production up to a time of 2e5 seconds. After this time, the production becomes constant until reach the well pressure.

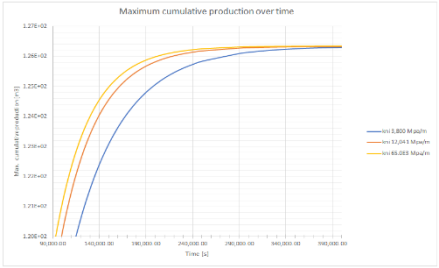

Figure 2. Maximum cumulative production over time for different k_{ni}. Source: author.

Figure 2 describes a lower maximum cumulative production for the k_{ni} of 3,800 MPa/m respect to the k_{ni} of 65,000 MPa/m. This means that a fracture with low stiffness (low k_{ni}) does not reach its maximum production compared to a fracture with a high stiffness, even if the simulation time is increased. So, a fracture with a low k_{ni} will tend to close faster than a fracture with a higher k_{ni}. Then, the geomechanical damage due to production will be characteristic and marked or low values of k_{ni}.

4.2 Local impact to the K_{ni} on the reservoir production

The local impact is studied as a function of the proximity of the well in the relation k_{ni} – fracture closure. Three fractures at different distances from the well were selected from the cell with 75 fractures. Figure 3b shows the first, second and third analyzed fractures located in the x direction of the well, approximately to 15 m, 30 m, and 70 m, respectively. Figure 3a and Fig. Figure 3b show the evolution of the fracture aperture over time as a function of k_{ni} for the fracture near to the well for Fracture 1 and Fracture 3, respectively. The fracture aperture is higher for k_{ni} = 65,000 MPa/m compared to the fracture aperture with k_{ni} = 3,800 MPa/m. This occurs because an open fracture has a direct relation with high values of k_{ni}.

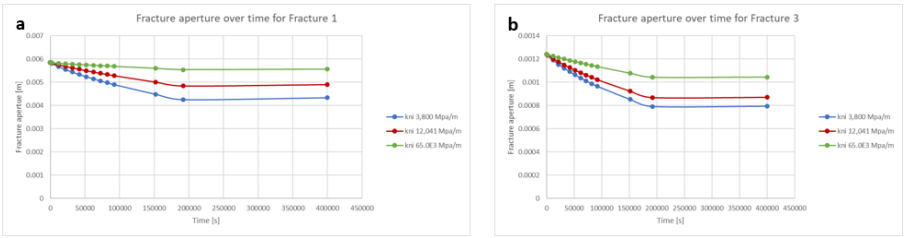

Figure 3. a- Fracture aperture over time for Fracture 1 as a function of different values of k_{ni}. Source: author. B- Fracture aperture over time for Fracture 3 as a function of different values of k_{ni}.

Figure 4 illustrates the variations of normal displacement of fracture closure over time for Fracture 1, Fracture 2 and Fracture 3 at a fixed k_{ni} of 12,041 MPa /m. Fracture 1 closure is greater compared to fracture 3 closure. Fracture 3 is the fracture farthest from the well and shows minimal closure over time. This occurs because the stress anisotropy decreases as a function of the distance from the well. Similar results were obtained the other k_{ni}. Then, it is possible to delimit a zone or damage radius in the areas near to the well. The impact of the k_{ni} on fracture aperture depends on closer to the well. Rodríguez [4], exposes the geomechanical formation damage due fracture closure occurs in the vicinity of the wellbore, up to about 3 ft away. The effective normal stress was calculated using Barton-Bandis model. Figure 4b and Fig. Figure 4c show the fracture closure variations as a function of the normal effective stress for the values of k_{ni}. The progressive increase of the closure fracture with the increase of the effective stresses due to the fluids production is evident for all these k_{ni}. Particularly, the fracture closure and normal effective stress are highest in Fracture 1 when k_{ni}= 3,800 MPa/m due to stress anisotropy near to the well, respect when k_{ni}= 65,000 MPa/m. Moreover, values of the normal effective stress on the Fracture 3 are less in all k_{ni} scenarios in comparison with Fracture 1.

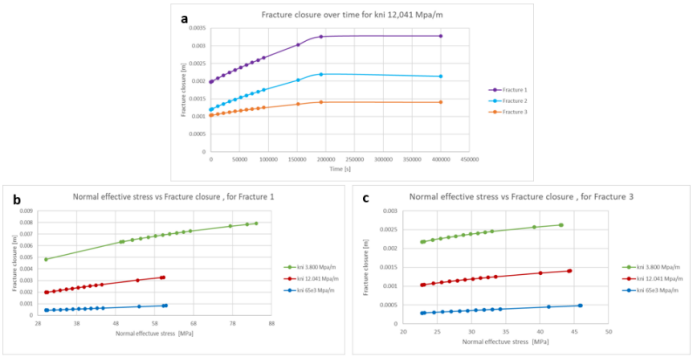

Figure 4. a- Fracture closure over time for Fracture 1, Fracture 2 and Fracture 3 with $k_{ni} = 12{,}041\ MPa/m$. b and c- Fracture closure variations as a function of normal effective stress for different values of k_{ni}, fracture 1 and Fracture 3, respectively.

5 Conclusions

The technique of embedded discontinuities applied in FEM let us to have a good approximation simulating the behavior of naturally fracture reservoir with the increase of confining stresses. At the same time, the

implementation of Barton-Bandis constitutive model was appropriate to analyze the relation between k_{ni} - fracture closure due stress change during production. The k_{ni} of the fractures impacts the deformability of the fracture during production. Thus, the k_{ni} of the fractures has a high impact on the maximum cumulative production of the reservoir. There is lower impact of the normal effective stress for a higher k_{ni} . The fracture closure is greater for fractures with less k_{ni} values respect to fractures with high k_{ni} values. However, although the fracture aperture is greater in the vicinity of the well, it is here where the greatest pressure drop occurs and, therefore, the greatest fracture closure, especially for fractures with low k_{ni}. The stress anisotropy decreases in the areas far from the well and high k_{ni}.

Authorship statement. The authors hereby confirm that they are the sole liable persons responsible for the authorship of this work, and that all material that has been herein included as part of the present paper is either the property (and authorship) of the authors or has the permission of the owners to be included here.

References

[1] J. Vigilio, G. Di Giulio, and L. Ferreira, "Not all glitters in the black gold: uncertainties and environmental threats of the brazilian Pre-salt," *Ambient. Soc.*, vol. 20, no. 3, pp. 21–38, 2017, [Online]. Available: http://www.scielo.br/pdf/asoc/v20n3/1809-4422-asoc-20-03-00021.pdf.

[2] V. Abdala, "La producción de petróleo supera 3 millones de barriles diarios," *Agência Brasil*, 2019. http://agenciabrasil.ebc.com.br/es/economia/noticia/2019-12/la-produccion-de-petroleo-supera-3-millones-de-barriles-diarios.

[3] E. Fjaer, R. M. Holt, P. Horsrud, A. M. Raaen, and R. Risnes, *Petroleum Related Rock Mechanics*, Second edi., vol. 1, no. 2. 2008.

[4] X. A. Rodríguez, "Daño geomecánico de sistemas naturalmente fracturados debido a esfuerzos inducidos por producción de fluidos," Universidad Nacional de Colombia - Sede Medellín, 2017.

[5] H. Buchsteiner and N. R. Warpinski, "Stress-Induced Permeability Reduction in Fissured Reservoirs," *Soc. Pet. Eng.*, vol. SPE 26513, no. October, pp. 65–74, 1993.

[6] M. Jin, J. Somerville, and B. G. Smart, "Coupled Reservoir Simulation Applied to the Management of Production Induced Stress-Sensitivity," *Soc. Pet. Eng.*, vol. SPE 64790, no. November, pp. 1–12, 2000.

[7] S. C. Bandis, A. C. Lumsden, and N. R. Barton, "Fundamentals of Rock Joint Deformation," *Int. J. Rock Mech. Min. Sci.*, vol. 20, no. 6, pp. 249–268, 1983.

[8] L. Yuting, D., Xudong, J., Yingfeng, M., y Pingya, "Closure Behaviour of Natural Rock Fractures," *Soc. Pet. Eng.*, vol. SPE 62539, no. June, pp. 1–9, 2000.

[9] L. Beserra, L. Guimarães, O. L. Manzoli, and L. Berrio, "Finite element with embedded discontinuities analysis of well production decline due to fracture closure in naturally fr," *16th Eur. Conf. Math. Oil Recover. ECMOR 2018*, no. September 2018, 2018, doi: 10.3997/2214-4609.201802156.

[10] F. Falcão *et al.*, "Synthetic benchmark for the computation of equivalent properties in coupled flow and geomechanics conditions for a fractured carbonate rock," *2nd Int. Discret. Fract. Netw. Eng. Conf. DFNE 2018*, 2018.

[11] O. L. Manzoli, M. A. Maedo, L. A. G. Bitencourt, and E. A. Rodrigues, "On the use of finite elements with a high aspect ratio for modeling cracks in quasi-brittle materials," *Eng. Fract. Mech.*, vol. 153, pp. 151–170, 2016, doi: 10.1016/j.engfracmech.2015.12.026.

[12] L. Beserra, "Análise hidromecânica do fraturamento hidráulico via elementos finitos com descontinuidades fortes incorporadas," 2015.

[13] S. Olivella, A. Gens, J. Carrera, and E. E. Alonso, "Numerical formulation for a simulator (CODE_BRIGHT) for the coupled analysis of saline media," *Eng. Comput.*, vol. 13, no. 7, pp. 87–112, 1996, doi: 10.1108/02644409610151575.

[14] L. D. N. Guimarães, A. Gens, and S. Olivella, "Coupled thermo-hydro-mechanical and chemical analysis of expansive clay subjected to heating and hydration," *Transp. Porous Media*, vol. 66, no. 3, pp. 341–372, 2007, doi: 10.1007/s11242-006-0014-z.

[15] L. L. Alvarez, L. Beserra, L. Guimarães, B. Maciel, and O. Manzoli, "Modeling of near - Wellbore permeability reduction due to depletion of a naturally fractured reservoir," *54th U.S. Rock Mech. Symp.*, 2020.

[16] L. Laura, A. Berrio, L. Brunet, D. S. Beserra, and F. Elements, "Study Case in a Naturally Fractured Reservoir During Depletion," pp. 151–160.